energies

MDPI

Article

Diffusion Characteristics of Dissolved Gases in Oil Under Different Oil Flow Circulations

Chuanxian Luo [1,2], Ye Zhu [1,2], Zhuangzhuang Li [3], Peng Yu [4], Zhengqin Zhou [1,2], Xu Yang [1,2] and Minfu Liao [4,*]

[1] NARI Group Corporation, State Grid Electric Power Research Institute, Nanjing 211000, China; luochuanxian@gepri.sgcc.com.cn (C.L.); zhuye@gepri.sgcc.com.cn (Y.Z.); zhouzhengqin@gepri.sgcc.com.cn (Z.Z.); yangxu@gepri.sgcc.com.cn (X.Y.)
[2] State Grid Electric Power Research Institute Wuhan Nari Co., Ltd., Wuhan 430074, China
[3] State Grid Shandong Electric Power Research Institute, Jinan 250021, China; lizhuangzhuang@sd.sgcc.com.cn
[4] School of Electrical Engineering, Dalian University of Technology, Dalian 116000, China; pyu@mail.dlut.cn
* Correspondence: lmf@dlut.edu.cn

Abstract: The prediction of dissolved gas concentrations in oil can provide crucial data for the assessment of power transformer conditions and early fault diagnosis. Current simulations mainly focus on the generation and accumulation of characteristic gases, lacking a global perspective on gas diffusion and dissolution. This study simulates the characteristic gases produced by typical faults at different flow rates. Using ANSYS 2022 R1 simulation software, a gas–liquid two-phase model is established to simulate the flow and diffusion of characteristic gases under fault conditions. Additionally, a fault-simulation gas production test platform was built based on a ±400 kV actual converter transformer. The experimental data show good consistency with the simulation trends. The results indicate that the diffusion of dissolved gases in oil is significantly affected by the oil flow velocity. At higher flow rates, the characteristic gases primarily move within the oil tank along with the oil circulation, leading to a faster rate of gas dissolution in oil and a shorter time to reach equilibrium within the tank. At lower flow rates, the diffusion of characteristic gases depends not only on oil flow circulation but also on self-diffusion driven by concentration gradients, resulting in a nonlinear change in gas concentration across various monitoring points.

Keywords: oil-immersed transformer; dissolved gas in oil; gas–liquid two-phase flow

Academic Editor: Anton Vernet

Received: 15 November 2024
Revised: 21 December 2024
Accepted: 25 December 2024
Published: 20 January 2025

Citation: Luo, C.; Zhu, Y.; Li, Z.; Yu, P.; Zhou, Z.; Yang, X.; Liao, M. Diffusion Characteristics of Dissolved Gases in Oil Under Different Oil Flow Circulations. *Energies* **2025**, *18*, 432. https://doi.org/10.3390/en18020432

1. Introduction

With the progressive development of the West–East Power Transmission Project, ultra-high-voltage (UHV) transmission technology has rapidly advanced [1–3]. As the core component of the transmission system, ensuring the safe and stable operation of UHV transformers remains a critical task in UHV transmission projects [4]. Currently, all UHV transformers are oil-immersed types, and to ensure their reliability, a variety of continuous monitoring technologies have been implemented [5,6]. Among these, dissolved gas analysis (DGA) monitoring technology stands out as the primary method due to its high accuracy, technical maturity, and resistance to field interference [7].

However, UHV transformers possess unique characteristics such as large size, complex structures, substantial oil volume, and extended gas transmission paths. In practical condition assessments, it has been observed that the characteristic values obtained from DGA monitoring cannot always accurately reflect the transformer's real-time operating status. This can lead to issues such as missed detections or false alarms. Therefore,

improving the accuracy of DGA monitoring to enable proactive and real-time condition alerts is of great practical significance for preventing serious transformer faults.

Currently, researchers worldwide are working to enhance the accuracy of DGA monitoring technology, primarily focusing on two approaches: algorithm-based prediction and simulation analysis. In the area of algorithm prediction, efforts are directed toward decomposing and reorganizing time-series data and optimizing them using advanced algorithms [8,9]. On the other hand, simulation studies have modeled gas diffusion concentrations at various fault points in two-dimensional transformer models, evaluating the effectiveness of monitoring points in detecting gas concentrations [10]. However, the dissolved gas content measured during DGA is only obtained after the gas has diffused to the sampling location, making the diffusion process a critical factor.

The large size and extended gas transmission paths of UHV transformers further complicate the understanding of how dissolved gases diffuse within the oil and are transported to monitoring points. Existing studies on this topic are limited and primarily focus on explaining the diffusion behavior of small gas molecules in insulation systems through microscopic molecular dynamics simulations [11,12]. Moreover, the complex structure and high cost of UHV transformers make it challenging and expensive to conduct experimental research simulating different defect types at typical fault locations in real-world transformers.

In summary, current research aimed at improving DGA monitoring accuracy is largely concentrated on processing monitoring data and optimizing monitoring systems. However, there is a lack of macro-level research on the diffusion process of dissolved gases in UHV transformers. To address this gap, this paper combines simulation analysis with experimental research to study the diffusion and distribution characteristics of dissolved gases generated by transformer faults under varying oil flow rates. By simulating the generation of characteristic gases at typical fault locations under different flow conditions, this study provides valuable insights for improving fault diagnosis based on dissolved gas monitoring technology.

2. Establishment of the Simulation Model

2.1. Simulation Model and Physical Parameters

The main focus of this paper is to investigate the diffusion and distribution characteristics of dissolved gases in oil in an oil-immersed transformer at different oil flow velocities. A fault simulation gas generation test platform was constructed based on a ±400 kV converter transformer from a specific substation. The physical diagram of the converter transformer is shown in Figure 1a. The converter transformer has a voltage rating of $535/\sqrt{3}/171.3$ kV, a complete internal structure, and a rated capacity of 363.4 MVA. A 1:1 scale simulation geometric model was constructed based on the physical diagram, as shown in Figure 1b. In order to simulate the occurrence of a fault at the position of the grid-side coil, the converter transformer was first pre-modified. An inlet for dissolved gas in oil was set up in the area of the neutral point lead of the grid-side winding of the converter transformer. One end of an 8-millimeter hose was extended into the neutral point lead. The installation and layout diagram of the oil guide pipe is shown in Figure 2.

In this simulation model, two lower oil ports serve as the inlet ports, while two upper oil ports function as the outlet ports. These upper and lower oil ports are interconnected. By setting different inlet port velocities in this simulation, the diffusion motion characteristics of dissolved gases in oil under different oil flow circulations are simulated. The fault point is set on the inner side of the grid-side coil. Since the flow velocity in the horizontal oil duct is relatively low, the influence of the horizontal oil duct is not considered in this paper. The interior of the converter transformer mainly consists of an iron core, a grid-side

winding, and a valve-side winding. As the voltage regulation winding is located closest to the iron core on the innermost side, it has little impact on the fluid flow. To reduce the unnecessary number of meshes and improve the mesh quality, it is ignored. The space between the windings is formed by narrow transformer barriers, which mainly serve to ensure the smooth flow of the oil path and prevent the formation of dead oil zones. Since this simulation focuses on the gas diffusion from a global perspective inside the converter transformer, they are ignored. The distances between the inner side of the valve-side winding and the outer side of the grid-side winding as well as between the inner side of the grid-side winding and the outer side of the iron core are 25 mm and 55 mm, respectively. Oil is the main medium inside the transformer, and its density and viscosity have a great impact on the convergence of the simulation calculation of fluid materials and the results. The type of transformer oil used in this experiment is KI25X, with a density of 886.8 kg/m^3 and a kinematic viscosity of 9.634 mm^2/s.

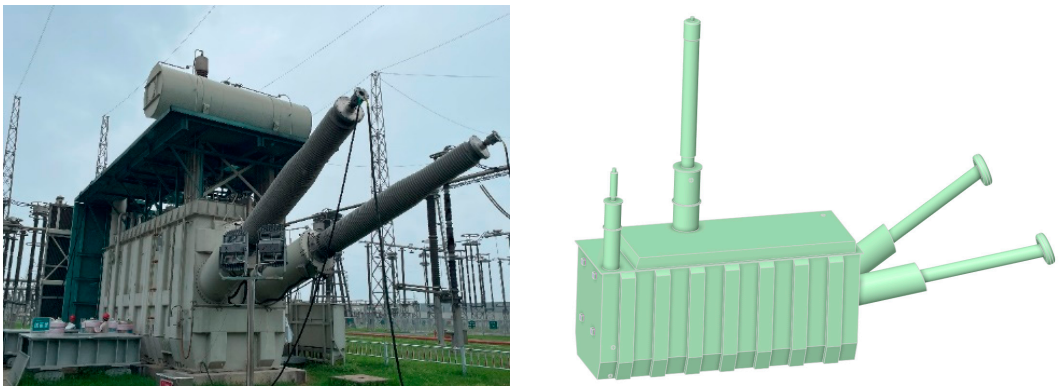

(**a**) (**b**)

Figure 1. Models of the ±400 kV converter transformer. (**a**) Actual geometric model; (**b**) simulation geometric model.

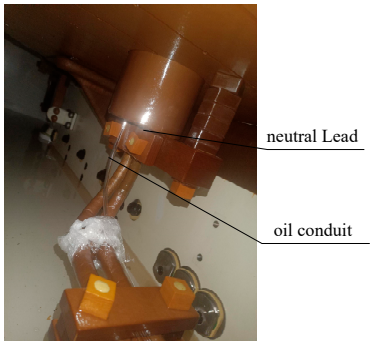

Figure 2. Oil injection pipe layout at the neutral lead point of the network-side winding.

Based on the established three-dimensional geometric model, a computational domain was constructed for the purpose of numerical simulation. Owing to the large scale and complex structure of the model, Ansys Mesh was employed to perform the meshing operation. The meshing model of the converter transformer is illustrated in Figure 3a. The grid independence analysis was conducted by analyzing the gas volume fraction at the monitoring points with varying numbers of grids. After a comprehensive evaluation, a grid consisting of 2,923,732 grid elements and 1,454,002 nodes was chosen. The orthogonal quality of all the grids was above 0.5, and there was no occurrence of negative volume. The verification result of grid independence is presented in Figure 3b. The model was solved using Fluent 2022R1, and the pressure–velocity coupling was resolved by the coupled SIMPLE algorithm. For the spatial discrete scheme, the gradient adopted the least square

method based on cell volume. The momentum, volume fraction, turbulent kinetic energy, turbulent dissipation, and dissolved gas all followed the first-order upwind format. The transient format was set as a first-order explicit format.

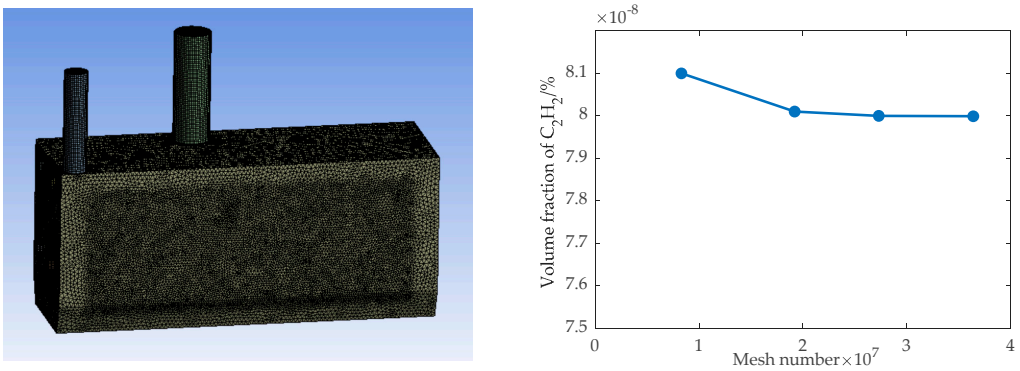

(**a**) (**b**)

Figure 3. (**a**) Mesh generation for the converter transformer; (**b**) verification of grid independence.

2.2. Control Equations

During the diffusion movement of dissolved gases within the transformer oil tank, characteristic gases are first generated at the fault location and dissolved into the oil, followed by diffusion throughout the tank. This study uses acetylene (C_2H_2) as a representative gas for testing. According to the fluid dynamics theory, the fluid motion behavior is described using the continuity equation and the Navier–Stokes equations:

$$\begin{cases} \frac{\partial \rho_l}{\partial t} + \nabla \cdot (\rho_l \mathbf{V}) = 0 \\ \rho_l \frac{\mathrm{d}\mathbf{V}}{\mathrm{d}t} = \rho_l g - \nabla p + \mu \nabla^2 \mathbf{V} \end{cases} \tag{1}$$

In these equations, ρ represents the fluid density (kg/m^3), v is the velocity vector (m/s), g denotes gravitational acceleration (m/s^2), p stands for fluid pressure (Pa), and μ is the dynamic viscosity of the fluid (Pa·s). In this paper, the gas injection point is located within the network-side coil, which is a relatively confined space with a high Reynolds number. Compared with the standard k-ε model and the RNG k-ε model, the realizable k-ε model introduces rotation and curvature effects. Additionally, it removes certain terms in the dissipation rate equation present in the turbulent kinetic energy equation, enhancing its suitability for this application. Therefore, this model can better describe the energy transfer process and has been applied to various types of complex flows, including jets, separated flows, and boundary layer flows. It demonstrates good stability, particularly for pipe flows at high Reynolds numbers.

$$-\rho\overline{u_i' u_j'} = \mu\left(\frac{\partial u_i}{\partial x_j} + \frac{\partial u_j}{\partial x_i}\right) - \frac{2}{3}\delta_{ij}\left(\rho k + \mu_t \frac{\partial u_i}{\partial x_i}\right) \tag{2}$$

$$\rho\frac{\mathrm{d}k}{\mathrm{d}t} = \frac{\partial}{\partial x_i}\left[\left(\mu + \frac{\mu_t}{\sigma_\mathrm{k}}\right)\frac{\partial k}{\partial x_i}\right] + G_\mathrm{k} + G_\mathrm{b} - \rho\varepsilon - Y_\mathrm{M} \tag{3}$$

$$\rho\frac{\mathrm{d}\varepsilon}{\mathrm{d}t} = \frac{\partial}{\partial x_i}\left[\left(\mu + \frac{\mu_\mathrm{t}}{\sigma_\varepsilon}\right)\frac{\partial \varepsilon}{\partial x_i}\right] + \rho C_1 S\varepsilon - \rho C_2 \frac{\varepsilon^2}{k + \sqrt{v\varepsilon}} + C_{1\varepsilon}\frac{\varepsilon}{k}C_{3c}G_\mathrm{b} \tag{4}$$

In the formula, $\overline{u_i}$ and u_i' (i = 1, 2, 3) are the mean velocity and the fluctuating velocity, respectively; δ_{ij} is the Kronecker delta; μ_i is the turbulent viscosity coefficient; G_k is the production term of turbulent kinetic energy k caused by the mean velocity gradient; G_b is the production term of turbulent kinetic energy caused by buoyancy, and

for incompressible fluids, $G_b = 0$; Y_M is the compressibility correction term, which is the contribution of the fluctuating expansion in compressible turbulence; S is the strain rate; $C_1 = \max[0.43, \eta/(\eta+5)]$; $\eta = (Sk)/\varepsilon$; and $C_{3\varepsilon}$ and $C_{2\varepsilon}$ are constants, where $C_{1\varepsilon} = 1.44$ and $C_{2\varepsilon} = 1.9$. For the flow in the same direction as the gravity direction, $C_{3\varepsilon} = 1$, and for the flow in the direction perpendicular to the gravity direction, $C_{3\varepsilon} = 0$; σ_k and σ_ε are the turbulent Prandtl numbers of turbulent kinetic energy and dissipation rate, respectively. Generally, $\sigma_k = 1$ and $\sigma_\varepsilon = 1.2$. $v = \mu/\rho$, which is the kinematic viscosity of the fluid, with the unit of m^2/s.

Regarding the research on gas diffusion characteristics in converter transformers, the focus is on the volume distribution of gas, and there is no requirement for the clarity of the gas–liquid interface. Therefore, the volume of fluid (VOF) model was excluded. The mixture model simplifies the interphase forces, reducing the amount of calculation. Moreover, if the forces between the two phases cannot be determined, using the Eulerian model may lead to inaccurate numerical calculation results. In this paper, the mixture model is used to simplify the diffusion process of dissolved gases in the oil, allowing different phases to penetrate each other and move at different velocities. The governing equations primarily include the continuity equation for the mixture phase, the momentum equation for the mixture, and the energy equation, as shown in Equations (5), (6), and (7), respectively.

$$\frac{\partial}{\partial t}(\rho m) + \nabla \cdot (\rho_m v_m) = m \tag{5}$$

$$\begin{aligned} \tfrac{\partial}{\partial t}(\rho_m v_m) + \nabla \cdot (\rho_m v_m v_m) &= -\nabla p + \nabla \cdot \left[\mu_m \left(\nabla v_m + \nabla v_m^T\right)\right] \\ &\quad + \rho_m g + F + \nabla \cdot \left(\sum_{k=1}^{n} \alpha_k \rho_k v_{dr,k} v_{dr,k}\right) \end{aligned} \tag{6}$$

$$\frac{\partial}{\partial t}\sum_{k=1}^{n}(\alpha_k \rho_k E_k) + \nabla \cdot \sum_{k=1}^{n}(\alpha_k v_k(\rho_k E_k + p)) = \nabla \cdot \left(k_{eff} \nabla T\right) + S_E \tag{7}$$

In the formula, m is the mass source term, representing the mass transfer amount in the phase change process; F is the body force ($m \cdot s^{-2}$); $V_{dr,k}$ is the slip velocity ($m \cdot s^{-1}$) of the k phase; k_{eff} is the effective thermal conductivity; and S_E is the energy source term, representing the energy absorbed or released during the phase change process.

3. Simulation Results and Analysis

3.1. Analysis of Simulation Results

This paper simulated a fault occurring at the grid-side coil for 20 s, accompanied by the generation of characteristic gas at a rate of 0.8 m/s. The monitoring time was set to 2 h, and the volume fraction of C_2H_2 at different monitoring points was observed.

As shown in Figure 4, when the oil flow velocity was 0.5 m/s, characteristic gas content was detected at monitoring point 4 starting from 3300 s, while all other monitoring points detected a change in characteristic gas at 1700 s. The dissolved gases in the oil at each monitoring point reached equilibrium by 5500 s. When the oil flow velocity was 1.5 m/s, monitoring points 1, 2, and 3 detected the characteristic gas starting at 400 s, while monitoring point 4 detected the characteristic gas content starting at 1000 s. Subsequently, the dissolved gases in the oil continued to diffuse with the oil flow circulation until they were completely dissolved in the oil tank and reached equilibrium. Monitoring point 5 reached equilibrium the earliest. It can be observed that as the oil flow velocity increased, the characteristic gas spread to the monitoring points more quickly. Since monitoring point 4 is located at the high-pressure casing, the oil flow circulation at this location was limited to the interface between the lower part of the raised seat and the main body of the oil tank.

As a result, the oil flow circulation was very slow, causing the detection of characteristic gas to occur later compared to the monitoring points located on the main body.

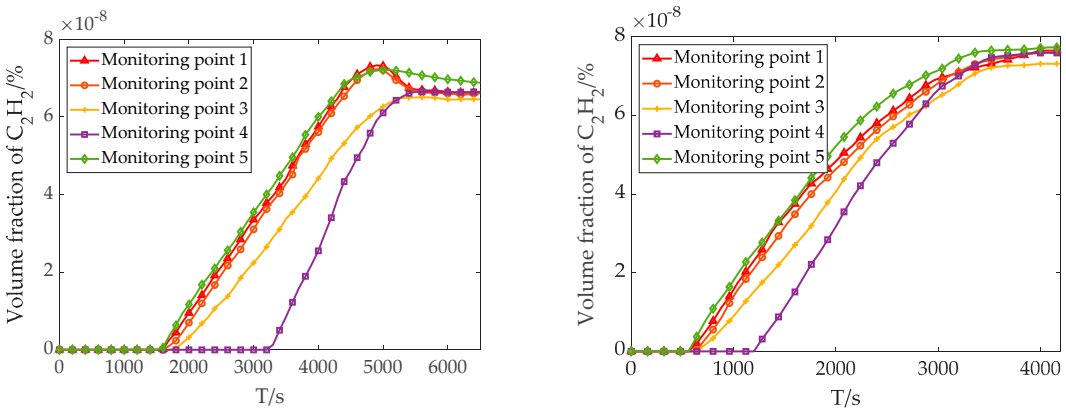

Figure 4. Variation of C_2H_2 volume fraction at different flow velocities: (**a**) v = 0.5 m/s; (**b**) v = 1.5 m/s.

3.2. Experimental Validation Analysis

The monitoring point positions in the experimental platform are consistent with those in the simulation model, as shown in Figure 5. Due to the large volume of transformer oil, long-duration real-time data collection and analysis were required during the experiment. Therefore, an acetylene online monitoring device was installed for the experiment. During the experiment, offline monitoring methods were combined with the simulation of fault gas generation. Oil samples were collected every 10 min during the fault simulation process, and then every 1 h thereafter. The ZF-301B instrument(Henan Zhongfen Instrument Co., Ltd., Shangqiu, China) was used to conduct offline chromatographic analysis on the oil samples. In the experiment, the acetylene online monitoring device analyzed the oil samples from each monitoring point every 30 min, and the results were compared and analyzed with the offline data.

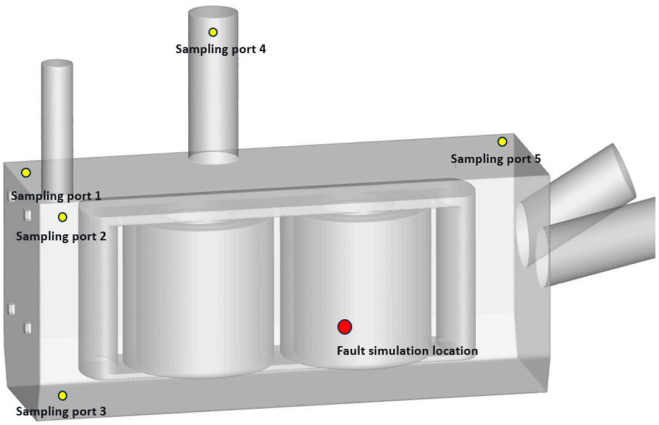

Figure 5. Schematic diagram of monitoring points and fault simulation location.

The experimental circuit diagram is shown in Figure 6. It mainly includes standard oil with a specific concentration, an oil pump, an oil flow velocity monitoring device, a liquid flowmeter, and the modified real transformer. In the experiment, the oil pump extracted the standard oil from the tank, and the liquid flowmeter was connected to control the injection rate and total amount of oil, which was then introduced into the grid-side coil of the converter transformer. To simulate the actual operating conditions of the converter

transformer and achieve the oil flow state under coil heating, low-frequency heating was used to raise the temperature of the transformer coil. The goal was to increase the top oil temperature of the converter transformer to approximately 50 °C and maintain this temperature throughout the experiment.

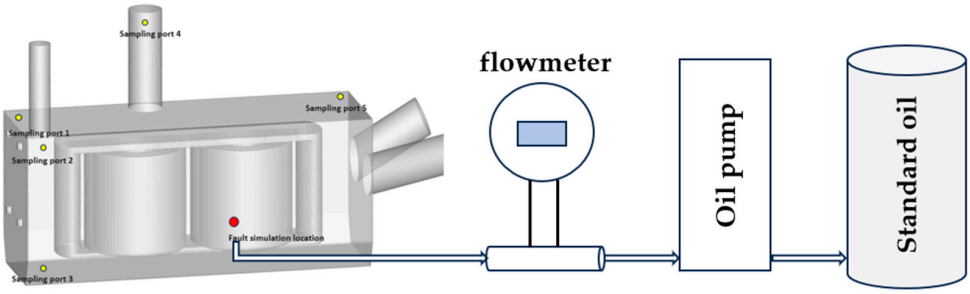

Figure 6. Experimental circuit diagram.

The experiment used the control of the cooling pump's operating quantity to change the oil flow circulation speed. The parameter settings for the experiment are shown in Table 1.

Table 1. Experimental parameter settings.

Serial Number	Fault Location	Fault Type	Standard Oil Concentration (ppm)	Injection Rate (m^3/h)	Number of Cooling Pumps	Injection Time (min)	Total Injection Amount (L)
1	Grid-side coil	Low energy	1600	0.1	1	60 min	200
2	Grid-side coil	Low energy	1600	0.1	3	60 min	200

In the experiment, the offline chromatographic data and online chromatographic data at the five monitoring points when three cooling pumps and one cooling pump were operating are shown in Figures 7 and 8, respectively.

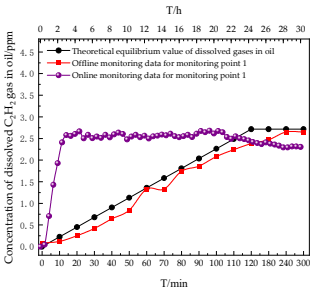

(**a**) Gas content at monitoring point 1

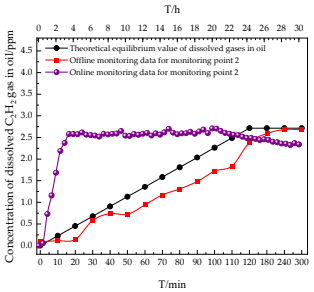

(**b**) Gas content at monitoring point 2

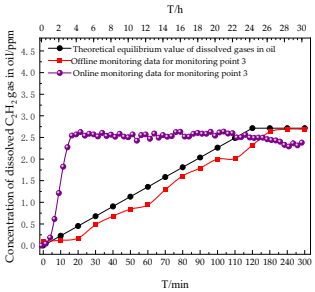

(**c**) Gas content at monitoring point 3

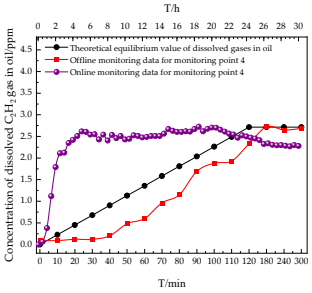

(**d**) Gas content at monitoring point 4

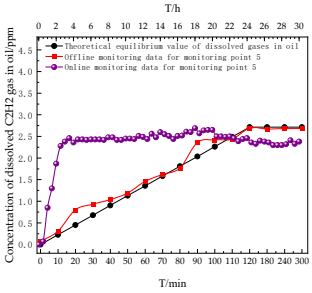

(**e**) Gas content at monitoring point 5

Figure 7. C_2H_2 concentration variation under three sets of oil pumps.

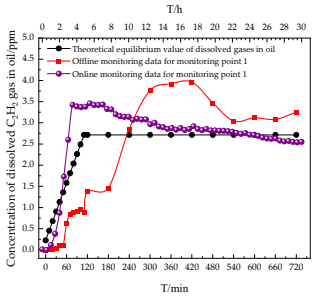

(**a**) Gas content at monitoring point 1

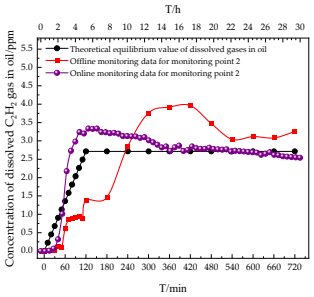

(**b**) Gas content at monitoring point 2

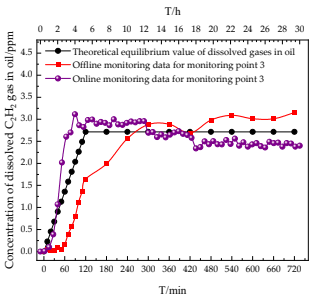

(**c**) Gas content at monitoring point 3

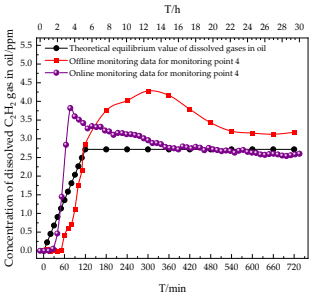

(**d**) Gas content at monitoring point 4

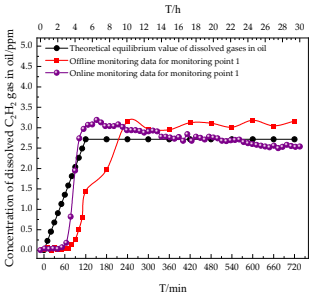

(**e**) Gas content at monitoring point 5

Figure 8. C_2H_2 concentration variation under one set of oil pumps.

From Figure 7, it can be observed that the monitoring points reached diffusion equilibrium around 180 min. Since monitoring points 1, 2, 3, and 5 are located on the main body of the transformer, gas concentration changes could be detected immediately after the start of the fault simulation, reaching equilibrium in approximately 20 min. In contrast, monitoring point 4, which is located on the elevated seat, exhibited a significant delay compared to the other monitoring points, reaching equilibrium at around 40 min. This delay occurred because the simulated fault is positioned on the transformer body. At the fault point, dissolved gases in the oil begin to generate at a certain speed under pressure. According to the Hagen–Poiseuille law, the formula is as follows:

$$\Delta P = \frac{8uLQ}{\pi r^4} \tag{8}$$

where ΔP is the pressure difference at different flow rates, u is the dynamic viscosity of the insulating oil, L is the length of the pipeline through which the insulating oil flows, Q is the flow rate, and r represents the radius of the characteristic gas generated by simulation.

It can be seen from (7) that the flow rate Q is directly proportional to ΔP. Since the flow rate Q is directly proportional to the flow velocity, the pressure difference is directly proportional to the flow velocity. In the experiment, the generation rate of the simulated characteristic gas was much lower than the flow rate of the insulating oil inside the transformer. This significant pressure difference between the two caused the flow direction of the characteristic gas to change. This is consistent with the results measured at monitoring points 1, 2, 3, and 5 on the transformer body, as shown in the figure. From the concentration changes at the five monitoring points in the figure, it can be observed that the concentration at the monitoring points located on the transformer body follows a nearly linear diffusion pattern. However, the concentration of dissolved gases at the monitoring point located on the raised seat exhibits a nonlinear diffusion pattern. Additionally, it can be seen that the concentration change gradient at the transformer body monitoring points closely matches the theoretical gradient.

As shown in the figure, the diffusion of dissolved gases with the same concentration in the oil inside the tank under one set of oil pumps is significantly different from the diffusion under three sets of cooling pumps. Furthermore, the concentration changes at all five monitoring points exhibit a nonlinear diffusion pattern. Since the oil flow circulation speed was slower at this point, the dissolved gases in the oil inside the tank did not reach equilibrium even after 720 min of offline monitoring. Additionally, it can be seen from the figure that the initial diffusion time was delayed, with the diffusion starting at 60 min. From the concentration change data at the monitoring points in the figure, it can be observed that a noticeable accumulation of dissolved gases generated by the fault occurred at each monitoring point. From the online data, it can be observed that after 14 h, the concentration of dissolved gases inside the oil tank reached diffusion equilibrium. As the monitoring time continued to increase, the concentration at the monitoring points began to show a decline. In the case of one cooling pump being activated, due to the slower oil flow speed, the pressure differential generated at the interface where the dissolved gases are produced at the fault location was greater than the oil flow velocity. As a result, the oil flow circulation was unable to promptly drive the diffusion movement of the dissolved gases in the oil. As the dissolved gases in the oil continued to be generated, a significant accumulation of dissolved gases occurred at the fault point. At this stage, the diffusion not only happened along with the oil flow circulation but also depended on the concentration difference between the dissolved gases in the oil and the blank oil.

From the above comparative analysis, it can be concluded that the experimental results are generally consistent with the simulation results. The simulation method is suitable for the gas–liquid two-phase flow motion simulation and analysis inside oil-immersed transformers. Due to the large model size and complex calculations during the simulation analysis, the fault gas generation set in the simulation is of a smaller order of magnitude compared to the settings in the experiment. As a result, there is a significant difference between the simulation and experimental results. Combining both the simulation and experimental results from a qualitative perspective, it is evident that the initial monitoring time for the characteristic gas at monitoring point 4 on the raised seat was significantly delayed compared to the other monitoring points. This is primarily because the oil flow circulation at the raised seat is limited to the interface between the lower part of the raised seat and the main body of the oil tank. As a result, the internal oil flow circulation is slower, causing a delay in the diffusion to monitoring point 4 compared to the monitoring points on the oil tank body. When the flow velocity is high, the diffusion of characteristic gases primarily depends on the oil flow circulation speed. However, when the flow velocity is low, the diffusion not only depends on the oil flow circulation but also occurs due to self-diffusion driven by the concentration difference. As a result, the diffusion reaching each monitoring point shows a nonlinear variation trend.

4. Conclusions

This study combined experiments and simulations to investigate the diffusion characteristics of dissolved gases in oil under different flow velocities, and the following conclusions are drawn:

(1) The diffusion of dissolved gases in oil is greatly influenced by the oil flow velocity. When the oil flow velocity is high, the characteristic gases mainly move within the oil tank along with the oil flow circulation. The gas dissolves into the oil at a faster rate, and equilibrium is reached more quickly within the oil tank. When the flow velocity is low, the diffusion of characteristic gases not only depends on the oil flow circulation but also occurs due to self-diffusion driven by the concentration difference. As a result, the diffusion reaching each monitoring point shows a nonlinear variation trend.

(2) Since the oil flow circulation at the raised seat monitoring point is limited to the interface between the lower part of the raised seat and the main body of the oil tank, the internal oil flow circulation speed is slower. As a result, the time for the dissolved gases to diffuse to monitoring point 4 is delayed compared to the monitoring points on the oil tank body at different oil flow velocities. Therefore, specific measures should be taken for faults occurring at the raised seat position, such as installing pressure sensors and other detection devices on the raised seat to monitor the pressure exerted by the insulating oil on the wall of the cylinder.

Author Contributions: C.L., Y.Z. and Z.L. proposed the idea for the paper; Z.Z. and X.Y. completed the numerical simulations; M.L. analyzed the data; P.Y. wrote the paper. All authors have read and agreed to the published version of the manuscript.

Funding: This work was supported in part by the State Grid Science and Technology Program under Grant 5108-202218280A-2-350-XG.

Data Availability Statement: The data presented in this study are available on request from the corresponding author due to (permission restriction).

Conflicts of Interest: Authors Chuanxian Luo, Ye Zhu, Zhengqin Zhou and Xu Yang were employed by the NARI Group Corporation and State Grid Electric Power Research Institute Wuhan Nari Co., Ltd. The remaining authors declare that the research was conducted in the absence of any commercial or financial relationships that could be construed as a potential conflict of interest.

References

1. Wang, H.; Zhang, Y.; Lin, W.; Wei, W. Transregional electricity transmission and carbon emissions: Evidence from ultra-high voltage transmission projects in China. *Energy Econ.* **2023**, *123*, 106751. [CrossRef]
2. Ma, L. Inter-provincial power transmission and its embodied carbon flow in China: Uneven green energy transition road to east and west. *Energies* **2021**, *15*, 176. [CrossRef]
3. Wang, Y.; Zhen, J.; Pan, H. Ultra-High-Voltage Construction Projects and Total Factor Energy Efficiency: Empirical Evidence on Cross-Regional Power Dispatch in China. *Sustainability* **2024**, *16*, 8083. [CrossRef]
4. Ali, M.S.; Omar, A.; Jaafar, A.S.A.; Mohamed, S.H. Conventional methods of dissolved gas analysis using oil-immersed power transformer for fault diagnosis: A review. *Electr. Power Syst. Res.* **2023**, *216*, 109064. [CrossRef]
5. Jin, L.; Kim, D.; Abu-Siada, A.; Kumar, S. Oil-immersed power transformer condition monitoring methodologies: A review. *Energies* **2022**, *15*, 3379. [CrossRef]
6. Soni, R.; Mehta, B. A review on transformer condition monitoring with critical investigation of mineral oil and alternate dielectric fluids. *Electr. Power Syst. Res.* **2023**, *214*, 108954. [CrossRef]
7. Jin, L.; Kim, D.; Chan, K.Y.; Abu-Siada, A. Deep Machine Learning-Based Asset Management Approach for Oil-Immersed Power Transformers Using Dissolved Gas Analysis. *IEEE Access* **2024**, *12*, 27794–27809. [CrossRef]
8. Zhang, G.; Chen, K.; Fang, R. Transformer fault diagnosis based on DGA and a whale algorithm optimizing a LogitBoost-decision tree. *Power Syst. Prot. Control.* **2023**, *51*, 63–72.
9. Xie, M.; Zhang, L.; Dong, X.; Xu, J. Prediction Method of Dissolved Gas Volume Fraction in Transformer Oil Based on OVMD-HWOA-KELM Model. *High Volt. Eng.* **2024**, *50*, 3793–3807.
10. Liu, R.; Wang, J.; Yu, Z.; Guo, Y. Research on Arrangement of Monitoring Points for Transformer Fault Characteristic Gases. *Transformer* **2023**, *60*, 27–33.
11. Cong, H.; Hu, X.; Du, Y.; Shao, H.; Li, Q. Micro-Mechanism Influence of Copper on Thermal Decomposition of Vegetable Oil-Paper Insulation Based on ReaxFF-MD. *IEEE Trans. Dielectr. Electr. Insul.* **2022**, *29*, 906–914. [CrossRef]
12. Liao, R.J.; Zhu, M.Z.; Zhou, X.; Yang, L.J.; Yan, J.M.; Sun, C.X. Molecular Dynamics Simulation of the Diffusion Behavior of Water Molecules in Oil and Cellulose Composite Media. *Acta Phys.-Chim. Sin.* **2011**, *27*, 815–824.